

High statistics measurement of the cross sections of $\gamma\gamma \rightarrow \pi^+\pi^-$ production

T. Mori,²² S. Uehara,⁸ Y. Watanabe,¹⁵ K. Abe,⁴² I. Adachi,⁸ H. Aihara,⁴⁴ K. Arinstein,¹ V. Aulchenko,¹ T. Aushev,^{18,50} A. M. Bakich,⁴⁰ V. Balagura,¹³ E. Barberio,²¹ A. Bay,¹⁸ K. Belous,¹² U. Bitenc,¹⁴ I. Bizjak,¹⁴ S. Blyth,²⁴ A. Bondar,¹ M. Bračko,^{8,20,14} T. E. Browder,⁷ M.-C. Chang,³ A. Chen,²⁴ W. T. Chen,²⁴ B. G. Cheon,⁶ I.-S. Cho,⁴⁹ S.-K. Choi,⁵ Y. Choi,³⁹ J. Dalseno,²¹ M. Dash,⁴⁸ A. Drutskoy,² S. Eidelman,¹ S. Fratina,¹⁴ N. Gabyshev,¹ B. Golob,^{19,14} H. Ha,¹⁶ K. Hayasaka,²² H. Hayashii,²³ M. Hazumi,⁸ D. Heffernan,³² T. Hokuue,²² Y. Hoshi,⁴² W.-S. Hou,²⁶ T. Iijima,²² K. Ikado,²² A. Imoto,²³ K. Inami,²² A. Ishikawa,⁴⁴ R. Itoh,⁸ M. Iwasaki,⁴⁴ Y. Iwasaki,⁸ H. Kaji,²² J. H. Kang,⁴⁹ P. Kapusta,²⁷ N. Katayama,⁸ T. Kawasaki,²⁹ H. Kichimi,⁸ H. O. Kim,³⁹ S. K. Kim,³⁷ Y. J. Kim,⁴ S. Korpar,^{20,14} P. Krizan,^{19,14} P. Krokovny,⁸ R. Kumar,³³ C. C. Kuo,²⁴ A. Kuzmin,¹ Y.-J. Kwon,⁴⁹ M. J. Lee,³⁷ S. E. Lee,³⁷ T. Lesiak,²⁷ J. Li,⁷ A. Limosani,⁸ S.-W. Lin,²⁶ D. Liventsev,¹³ J. MacNaughton,¹¹ F. Mandl,¹¹ T. Matsumoto,⁴⁶ A. Matyjka,²⁷ S. McOnie,⁴⁰ T. Medvedeva,¹³ H. Miyake,³² H. Miyata,²⁹ Y. Miyazaki,²² R. Mizuk,¹³ G. R. Moloney,²¹ Y. Nagasaka,⁹ E. Nakano,³¹ M. Nakao,⁸ H. Nakazawa,²⁴ Z. Natkaniec,²⁷ S. Nishida,⁸ O. Nitoh,⁴⁷ S. Noguchi,²³ T. Ohshima,²² S. Okuno,¹⁵ S. L. Olsen,⁷ S. Ono,⁴⁵ Y. Onuki,³⁵ W. Ostrowicz,²⁷ H. Ozaki,⁸ P. Pakhlov,¹³ G. Pakhlova,¹³ C. W. Park,³⁹ H. Park,¹⁷ K. S. Park,³⁹ R. Pestotnik,¹⁴ L. E. Pilonen,⁴⁸ A. Poluektov,¹ H. Sahoo,⁷ Y. Sakai,⁸ N. Satoyama,³⁸ O. Schneider,¹⁸ J. Schümann,⁸ K. Senyo,²² M. E. Sevier,²¹ M. Shapkin,¹² C. P. Shen,¹⁰ H. Shibuya,⁴¹ B. Shwartz,¹ J. B. Singh,³³ A. Sokolov,¹² A. Somov,² N. Soni,³³ S. Stanič,³⁰ M. Starič,¹⁴ H. Stoeck,⁴⁰ T. Sumiyoshi,⁴⁶ S. Y. Suzuki,⁸ F. Takasaki,⁸ K. Tamai,⁸ M. Tanaka,⁸ G. N. Taylor,²¹ Y. Teramoto,³¹ X. C. Tian,³⁴ I. Tikhomirov,¹³ T. Tsuboyama,⁸ T. Tsukamoto,⁸ K. Ueno,²⁶ T. Uglov,¹³ Y. Unno,⁶ S. Uno,⁸ P. Urquijo,²¹ Y. Usov,¹ G. Varner,⁷ K. Vervink,¹⁸ S. Villa,¹⁸ A. Vinokurova,¹ C. H. Wang,²⁵ P. Wang,¹⁰ E. Won,¹⁶ Q. L. Xie,¹⁰ B. D. Yabsley,⁴⁰ A. Yamaguchi,⁴³ Y. Yamashita,²⁸ C. C. Zhang,¹⁰ Z. P. Zhang,³⁶ V. Zhilich,¹ V. Zhulanov,¹ and A. Zupanc¹⁴

(The Belle Collaboration)

¹*Budker Institute of Nuclear Physics, Novosibirsk*

²*University of Cincinnati, Cincinnati, Ohio 45221*

³*Department of Physics, Fu Jen Catholic University, Taipei*

⁴*The Graduate University for Advanced Studies, Hayama*

⁵*Gyeongang National University, Chinju*

⁶*Hanyang University, Seoul*

⁷*University of Hawaii, Honolulu, Hawaii 96822*

⁸*High Energy Accelerator Research Organization (KEK), Tsukuba*

⁹*Hiroshima Institute of Technology, Hiroshima*

¹⁰*Institute of High Energy Physics, Chinese Academy of Sciences, Beijing*

¹¹*Institute of High Energy Physics, Vienna*

¹²*Institute of High Energy Physics, Protvino*

¹³*Institute for Theoretical and Experimental Physics, Moscow*

¹⁴*J. Stefan Institute, Ljubljana*

¹⁵*Kanagawa University, Yokohama*

¹⁶*Korea University, Seoul*

¹⁷*Kyungpook National University, Taegu*

¹⁸*Swiss Federal Institute of Technology of Lausanne, EPFL, Lausanne*

¹⁹*University of Ljubljana, Ljubljana*

²⁰*University of Maribor, Maribor*

²¹*University of Melbourne, School of Physics, Victoria 3010*

²²*Nagoya University, Nagoya*

²³*Nara Women's University, Nara*

²⁴*National Central University, Chung-li*

- ²⁵*National United University, Miao Li*
²⁶*Department of Physics, National Taiwan University, Taipei*
²⁷*H. Niewodniczanski Institute of Nuclear Physics, Krakow*
²⁸*Nippon Dental University, Niigata*
²⁹*Niigata University, Niigata*
³⁰*University of Nova Gorica, Nova Gorica*
³¹*Osaka City University, Osaka*
³²*Osaka University, Osaka*
³³*Panjab University, Chandigarh*
³⁴*Peking University, Beijing*
³⁵*RIKEN BNL Research Center, Upton, New York 11973*
³⁶*University of Science and Technology of China, Hefei*
³⁷*Seoul National University, Seoul*
³⁸*Shinshu University, Nagano*
³⁹*Sungkyunkwan University, Suwon*
⁴⁰*University of Sydney, Sydney, New South Wales*
⁴¹*Toho University, Funabashi*
⁴²*Tohoku Gakuin University, Tagajo*
⁴³*Tohoku University, Sendai*
⁴⁴*Department of Physics, University of Tokyo, Tokyo*
⁴⁵*Tokyo Institute of Technology, Tokyo*
⁴⁶*Tokyo Metropolitan University, Tokyo*
⁴⁷*Tokyo University of Agriculture and Technology, Tokyo*
⁴⁸*Virginia Polytechnic Institute and State University, Blacksburg, Virginia 24061*
⁴⁹*Yonsei University, Seoul*
⁵⁰*Institute for Theoretical and Experimental Physics, Moscow*
(Dated: April 5, 2007)

We report on a high statistics measurement of the total and differential cross sections of the process $\gamma\gamma \rightarrow \pi^+\pi^-$ in the $\pi^+\pi^-$ invariant mass range $0.8 \text{ GeV}/c^2 < W < 1.5 \text{ GeV}/c^2$ with 85.9 fb^{-1} of data collected at $\sqrt{s} = 10.58 \text{ GeV}$ and 10.52 GeV with the Belle detector. A clear signal of the $f_0(980)$ resonance is observed in addition to the $f_2(1270)$ resonance. An improved 90% confidence level upper limit $\mathcal{B}(\eta'(958) \rightarrow \pi^+\pi^-) < 2.9 \times 10^{-3}$ is obtained for P - and CP -violating decay of the $\eta'(958)$ meson using the most conservative assumption about the interference with the background.

KEYWORDS: two-photon production, $f_0(980)$, $f_2(1270)$, $\eta'(958)$, $\gamma\gamma \rightarrow \pi^+\pi^-$ cross section

I. INTRODUCTION

The nature of low mass mesons remains poorly understood in spite of decades of theoretical and experimental effort [1]. In particular, low mass scalar mesons (below $1 \text{ GeV}/c^2$) are not yet well established experimentally except for the $f_0(980)$ and $a_0(980)$ mesons, while the extensively discussed σ ($f_0(600)$) and κ ($K^*(800)$) mesons still remain controversial states [2]. A B factory is well suited for detailed investigations of low mass mesons through two-photon production, where overwhelming statistics can be obtained. Two-photon production of mesons has advantages over meson production in hadronic processes; the production rate can be reliably calculated from QED with $\Gamma_{\gamma\gamma}$ as the only unknown parameter. In addition, a meson can be produced alone without additional hadronic debris, and the quantum numbers of the final state are restricted to states of charge conjugation $C = +1$ with $J = 1$ forbidden (Landau-Yang's theorem [3]).

In the past, extensive studies of low mass mesons through $\gamma\gamma \rightarrow \pi\pi$ scattering have been made at e^+e^- colliders: Crystal Ball [4], Mark II [5], JADE [6], TOPAZ [7], MD-1 [8], CELLO [9] and VENUS [10]; see Ref. [2] for a list of the earlier experiments. Using data from Mark II, Crystal Ball, and CELLO, Boglione and Pennington (BP) performed an amplitude analysis of $\gamma\gamma \rightarrow \pi^+\pi^-$ and $\gamma\gamma \rightarrow \pi^0\pi^0$ cross sections [11]. They found two distinct classes

of solutions where one solution has a peak (“peak” solution) and the other has a wiggle (“dip” solution) in the $f_0(980)$ mass region. The two solutions give quite different results for the two-photon width of the $f_0(980)$ and the size of the S-wave component. Thus, it is necessary to distinguish them experimentally.

In this paper, we report on a measurement of the cross sections for the reaction $\gamma\gamma \rightarrow \pi^+\pi^-$ with high statistics that are more than two orders of magnitude larger than that of the past experiments. The analysis is based on data taken with the Belle detector at the KEKB asymmetric-energy (3.5 GeV on 8 GeV) e^+e^- collider [12]. The data sample corresponds to a total integrated luminosity of 85.9 fb^{-1} , accumulated on the $\Upsilon(4S)$ resonance ($\sqrt{s} = 10.58 \text{ GeV}$) and 60 MeV below the resonance (8.6 fb^{-1} of the total). Since the cross section difference between the two energies is only about 0.3%, we combine both samples [13]. We observe the two-photon process $e^+e^- \rightarrow e^+e^-\pi^+\pi^-$ in the “zero-tag” mode, where neither the final-state electron nor positron is detected, and the $\pi^+\pi^-$ system has small transverse momentum. We restrict the virtuality of the incident photons to be small by imposing a strict requirement on the transverse-momentum balance of the final-state hadronic system with respect to the beam axis. Some of the results reported here are the subject of a separate paper focusing on the properties of the $f_0(980)$ meson [14].

This paper is organized as follows. A brief description of the detector is given in section II. The selection criteria are listed in section III. There is a well known difficulty in discriminating μ^\pm from π^\pm in the low momentum region ($\lesssim 0.8 \text{ GeV}/c$); Section IV presents the method of particle identification, in particular the method of μ/π separation that we use. Evaluation of the detection and trigger efficiencies is described in section V. The total and differential cross sections are given while their systematic errors are estimated in section VI. In section VII, the resulting spectrum is fitted to obtain the resonance parameters of the $f_0(980)$ meson and to check consistency in the $f_2(1270)$ region. Section VIII summarizes the results. Appendix A gives a detailed description of the background subtraction. Values of the total cross sections are given in Appendix B.

II. THE BELLE DETECTOR

The Belle detector is a large-solid-angle magnetic spectrometer having good momentum resolution and particle identification capability in the energy region of interest [15]. Here we briefly describe the Belle detector components. Charged track coordinates near the collision point are measured by a 3-layer silicon vertex detector (SVD) that surrounds a 2 cm radius beryllium beam pipe. Track trajectories are reconstructed in a 50-layer central drift chamber (CDC), and momentum measurements are made together with the SVD. An array of 1188 silica-aerogel Cherenkov counters (ACC) provides separation between kaons and pions for momenta above $1.2 \text{ GeV}/c$. The time-of-flight counter (TOF) system consists of a barrel of 128 plastic scintillation counters and is effective for K/π separation for tracks with momenta below $1.2 \text{ GeV}/c$. Low energy kaons and protons are also identified through specific ionization (dE/dx) measurements in the CDC. Photon detection and energy measurements of photons and electrons are provided by an electromagnetic calorimeter (ECL). It is comprised of an array of 8736 CsI(Tl) crystals all pointed toward the interaction point, greatly enhances the electron identification capability provided through a comparison of energy measured in the ECL and momentum in the CDC. These detector components are located within a superconducting solenoid coil that provides a uniform magnetic field of 1.5 T. An iron flux-return located outside the solenoid coil is instrumented to detect K_L^0 mesons and to identify muons (KLM). The z axis of the detector is defined to be opposite to the direction of the positron beam. These detector components cover a polar angular range between 17° and 150° .

III. EVENT SELECTION

Signal candidates are primarily triggered by a two-track trigger that requires two CDC tracks with associated TOF hits and ECL clusters with an opening angle greater than 135° . Exclusive $e^+e^- \rightarrow e^+e^-\pi^+\pi^-$ events are selected by requiring two oppositely charged tracks coming from the interaction region; each track is required to satisfy $dr < 0.1$ cm and $|dz| < 2$ cm, where dr (dz) is r (z) component of the closest approach to the nominal collision point. Here, r is the transverse distance from the z axis. The difference of the dz 's of the two tracks must satisfy the requirement $|dz_+ - dz_-| \leq 1$ cm. The event must contain one and only one positively charged track that satisfies $p_t > 0.3$ GeV/ c and $-0.47 < \cos\theta < 0.82$, where p_t and θ are the transverse component of momentum and the angle with respect to the z -axis. The scalar sum of the track momenta in each event is required to be less than 6 GeV/ c , and the sum of the ECL energies of the event must be less than 6 GeV. Events should not include an extra track with $p_t > 0.1$ GeV/ c . The cosine of the opening angle of the tracks must be greater than -0.997 to reject cosmic-ray events. The sum of transverse momentum vectors of the two tracks ($\sum \mathbf{p}_t^*$) should satisfy $|\sum \mathbf{p}_t^*| < 0.1$ GeV/ c ; this requirement separates exclusive two-track events from quasi-real two-photon collisions.

IV. PARTICLE IDENTIFICATION AND μ/π SEPARATION

Electrons and positrons are clearly distinguished from hadrons using the ratio E/p , where E is the energy measured in the ECL, and p is the momentum from the CDC. Kaon (proton) candidates are identified using normalized kaon (proton) and pion likelihood functions (L_K (L_p) and L_π , respectively) obtained from the particle identification system (combining the information of the CDC, TOF, ACC and ECL) with the criterion $L_K/(L_K + L_\pi) > 0.25$ ($L_p/(L_p + L_\pi) > 0.5$), which gives a typical identification efficiency of 90% with a pion misidentification probability of 3%. All charged tracks that are not identified as electrons, kaons or protons are treated as pions. We require both tracks to be pions. The resulting invariant mass (W) distribution is shown in Fig. 1. The W bin size is chosen to be 5 MeV/ c^2 , while the mass resolution is about 2 MeV/ c^2 according to GEANT-3 [16] based Monte Carlo (MC) simulation. A clear signal corresponding to the $f_0(980)$ meson is seen along with the well known $f_2(1270)$ resonance.

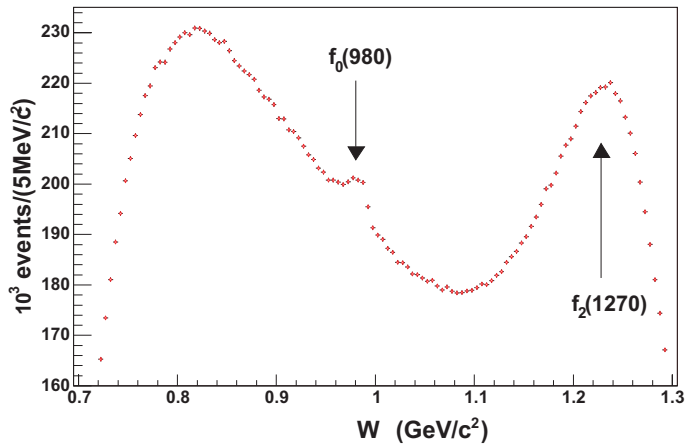


FIG. 1: The invariant mass distribution of unseparated ($\mu^+\mu^- + \pi^+\pi^-$) events. A clear signal for the $f_0(980)$ can be seen. The large peak around $W = 1.2$ GeV/ c^2 corresponds to the $f_2(1270)$ resonance. Note the suppressed zero on the vertical scale.

In this measurement, the KLM detector cannot be used for muon identification, since it is insensitive in the region of interest where the transverse momenta of tracks are below $0.8 \text{ GeV}/c$. Therefore, we have developed a method for separating $\pi^+\pi^-$ and $\mu^+\mu^-$ events statistically using ECL information; muons deposit energy corresponding to the ionization loss for minimum ionizing particles, while pions give a wider energy distribution since they may interact hadronically in the ECL, which corresponds to approximately one interaction length of material. Typical two-dimensional distributions (E_+ vs. E_-) of the energy deposit E_{\pm} in the ECL for $\mu^+\mu^-$ and $\pi^+\pi^-$ pairs produced by MC are shown in Figs. 2(a) and 2(b).

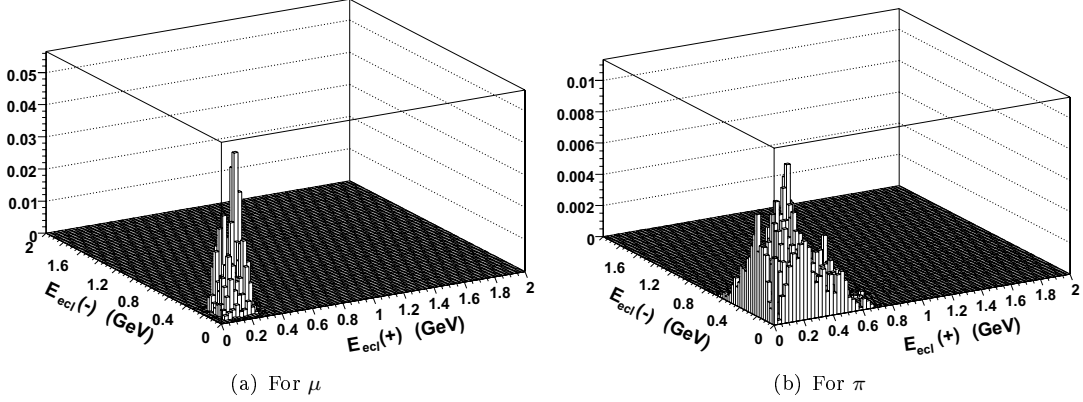


FIG. 2: Typical distributions of the energy deposit (E_+ vs. E_-) in the ECL. Events are produced using MC simulation in a range $1.0 \text{ GeV}/c^2 < W < 1.02 \text{ GeV}/c^2$ and $|\cos \theta^*| < 0.1$.

Probability density functions (PDFs) for the distributions of energy deposits from $\pi^+\pi^-$ ($\mu^+\mu^-$) pairs $P_{\pi^+\pi^-}^{(i)}(E_+, E_-)$ ($P_{\mu^+\mu^-}^{(i)}(E_+, E_-)$) are obtained with MC simulation. Here i represents the i -th bin of $(W, |\cos \theta^*|)$ in $20 \text{ MeV}/c^2$ and 0.1 steps, where W is the invariant mass of the $\pi^+\pi^-$ (or $\mu^+\mu^-$) pair in each event (the pion mass is assumed in the calculation), and θ^* is the polar angle of the produced π^\pm meson (or μ^\pm lepton) in the center-of-mass system of two initial photons. Note that using this method the effect of muons from pion decays is taken into account by the pion PDFs. We obtain $r^{(i)}$, the fraction of $\mu^+\mu^-$ in the i -th bin through the equation:

$$N_{\text{data}}^{(i)}(E_+, E_-) = N_{\text{tot}}^{(i)} \left(r^{(i)} P_{\mu^+\mu^-}^{(i)}(E_+, E_-) + (1 - r^{(i)}) P_{\pi^+\pi^-}^{(i)}(E_+, E_-) \right), \quad (1)$$

where $N_{\text{data}}^{(i)}(E_+, E_-)$ is the distribution of data and $N_{\text{tot}}^{(i)}$ is the total number of events in that bin. The values of ratios $r^{(i)}$ obtained must be corrected since the MC cannot simulate hadronic interactions accurately enough. By introducing mis-ID probabilities, $P_{\pi\pi \rightarrow \mu\mu}$ and $P_{\mu\mu \rightarrow \pi\pi}$, the r value for each bin (the bin number i is omitted) can be written as:

$$r = \frac{N_{\mu\mu} + N_{\pi\pi} P_{\pi\pi \rightarrow \mu\mu} - N_{\mu\mu} P_{\mu\mu \rightarrow \pi\pi}}{N_{\mu\mu} + N_{\pi\pi}}, \quad (2)$$

where $N_{\pi\pi}$ ($N_{\mu\mu}$) is the number of true $\pi^+\pi^-$ ($\mu^+\mu^-$) pairs in that bin. We assume that $P_{\pi\pi \rightarrow \mu\mu}$ and $P_{\mu\mu \rightarrow \pi\pi}$ are independent of W . Applying the μ/π separation method mentioned above to a sample of data events positively identified as muons by the KLM information in the higher energy region, we find that $P_{\mu\mu \rightarrow \pi\pi}$ is statistically consistent with zero. The values of $P_{\pi\pi \rightarrow \mu\mu}$ in each $|\cos \theta^*|$ bin are determined such that the ratio of the data and MC for $\mu^+\mu^-$ pairs, which is ideally one, gives a straight line in the W spectrum. The values of $P_{\pi\pi \rightarrow \mu\mu}$ vary between 0.08 to 0.13 in $|\cos \theta^*|$ bins. Because they are determined

for each bin of $|\cos\theta^*|$, the bin-by-bin variation of systematic errors is rather large in the angular distribution. After subtracting $\mu^+\mu^-$ events, a total of 6.4×10^6 events remains in the region of $0.8 \text{ GeV}/c^2 < W < 1.5 \text{ GeV}/c^2$ and $|\cos\theta^*| < 0.6$.

V. DETECTION AND TRIGGER EFFICIENCY

The detection (trigger) efficiencies, ϵ_{det} (ϵ_{trg}) are estimated from a MC simulation. Events of the process $\gamma\gamma \rightarrow \pi^+\pi^-$ are generated using TREPS [17]. The detection efficiency is calculated from the MC simulation as the ratio of the number of detected and generated events in each bin of W (with the bin width, $5 \text{ MeV}/c^2$) and $|\cos\theta^*|$ (0.05). The MC statistics are high enough and do not contribute to systematic errors.

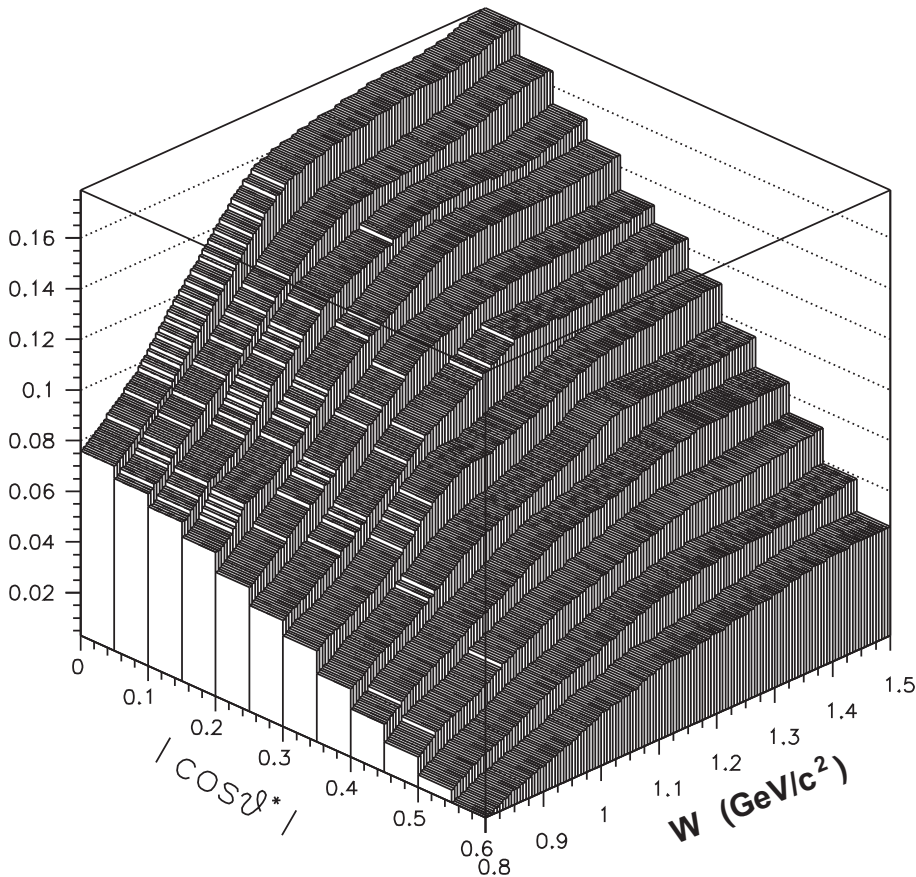


FIG. 3: The combined detection and trigger efficiencies as a function of W and $|\cos\theta^*|$.

The trigger efficiencies are estimated with the same binning using the trigger simulator. Since the trigger simulator does not simulate triggers very accurately, particularly in the low energy region, the efficiency values have to be corrected. We calculate the correction factors by comparing the number of $e^+e^- \rightarrow e^+e^-e^+e^-$ events in data and MC that are triggered by the two-track trigger. The resulting factors steeply rise from 0.5 at $W = 0.8 \text{ GeV}/c^2$ to 0.8 at $W = 1 \text{ GeV}/c^2$ and then increase gradually for higher W . The combined detection and trigger efficiencies are shown in Fig. 3. The muon-background subtraction and all the correction factors are applied using smooth functions obtained by parameterizing the results of bin-by-bin analyses.

VI. CROSS SECTIONS

In this section, we derive differential and total cross sections and evaluate systematic errors.

A. Differential Cross Sections

Differential cross sections for $\gamma\gamma \rightarrow \pi^+\pi^-$ are evaluated by using the following relation:

$$\frac{\Delta\sigma_{\gamma\gamma \rightarrow \pi^+\pi^-}}{\Delta|\cos\theta^*|} = \frac{\Delta N_{e^+e^- \rightarrow e^+e^-\pi^+\pi^-}}{\epsilon_{\text{trg}} \cdot \epsilon_{\text{det}} \cdot \Delta W \cdot \Delta|\cos\theta^*| \cdot \frac{d\mathcal{L}}{dW} \cdot \int Ldt}, \quad (3)$$

where $\Delta N_{e^+e^- \rightarrow e^+e^-\pi^+\pi^-}$ is the number of events in a W - $|\cos\theta^*|$ bin, $\frac{d\mathcal{L}}{dW}$ is the two-photon luminosity function [18] and $\int Ldt = 85.9 \text{ fb}^{-1}$ is the integrated luminosity. Here the W and $|\cos\theta^*|$ bin sizes are also chosen to be $5 \text{ MeV}/c^2$ and 0.05 , respectively. Background from $\eta'(958) \rightarrow \rho^0\gamma \rightarrow \pi^+\pi^-\gamma$ is subtracted, a detailed account of which is given in Appendix A. The contribution of the background to the cross section is about 5% at $0.8 \text{ GeV}/c^2$ and dies away quickly to zero above $0.9 \text{ GeV}/c^2$. Other backgrounds are negligible.

Differential cross sections $d\sigma/d|\cos\theta^*|$ are obtained using Eq. (3) for $|\cos\theta^*|$ from 0 to 0.6 and for W from $0.8 \text{ GeV}/c^2$ up to $1.5 \text{ GeV}/c^2$. The resulting differential cross sections are shown in Fig. 4. In order to present the cross sections more quantitatively, some representative ones are also plotted in Fig. 5. Both statistical and point-by-point errors are shown. The latter come from the μ/π separation method and trigger efficiency corrections we employ as explained in Sections IV and V. A point-by-point systematic error is taken to be one half of the difference between the corrections in neighboring bins. The result shows some apparent systematic structure in the region $0.45 < |\cos\theta^*| < 0.6$, particularly for $W < 1.1 \text{ GeV}/c^2$. As shown below (see Eq. (4)), the differential cross sections in this W region can be described by a second order polynomial in $|\cos\theta^*|^2$. Thus, such structures are not considered to be real; either the last points are too low or earlier points are too high. However, we have not identified the cause of the measurement bias.

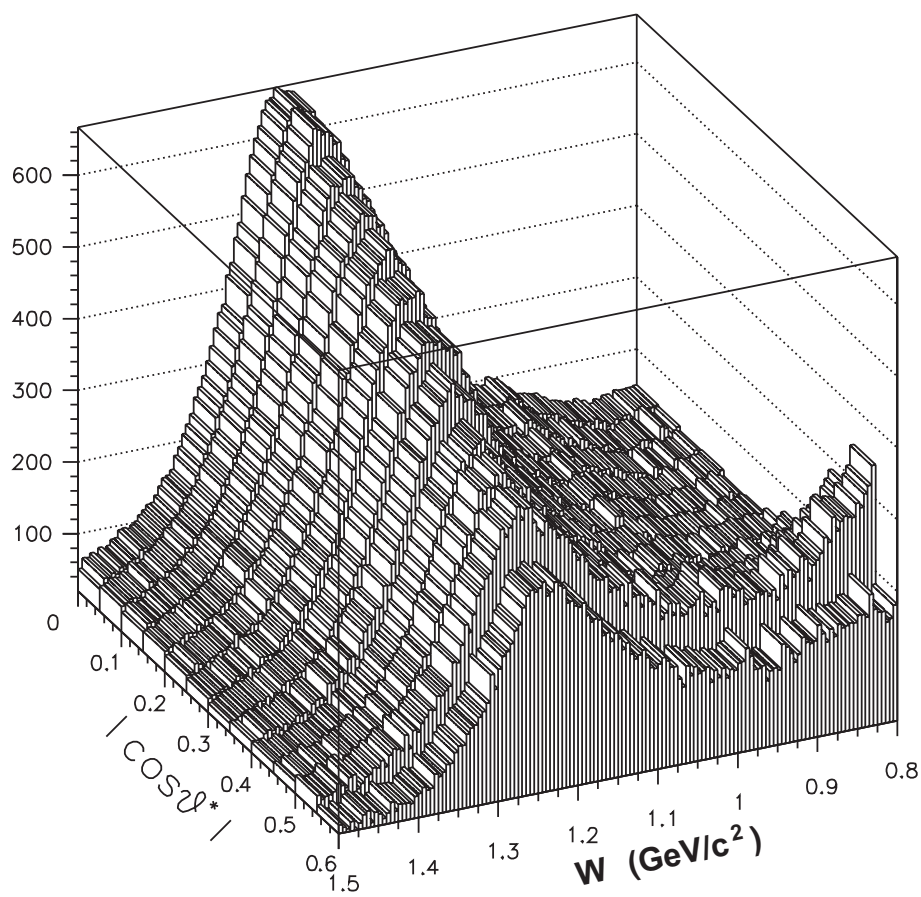


FIG. 4: Differential cross sections ($d\sigma/d|\cos\theta^*|$ (nb)). (The W -axis is reversed compared to that of Fig. 3 so as to allow a clearer view of the region in W above the $f_2(1270)$ resonance.)

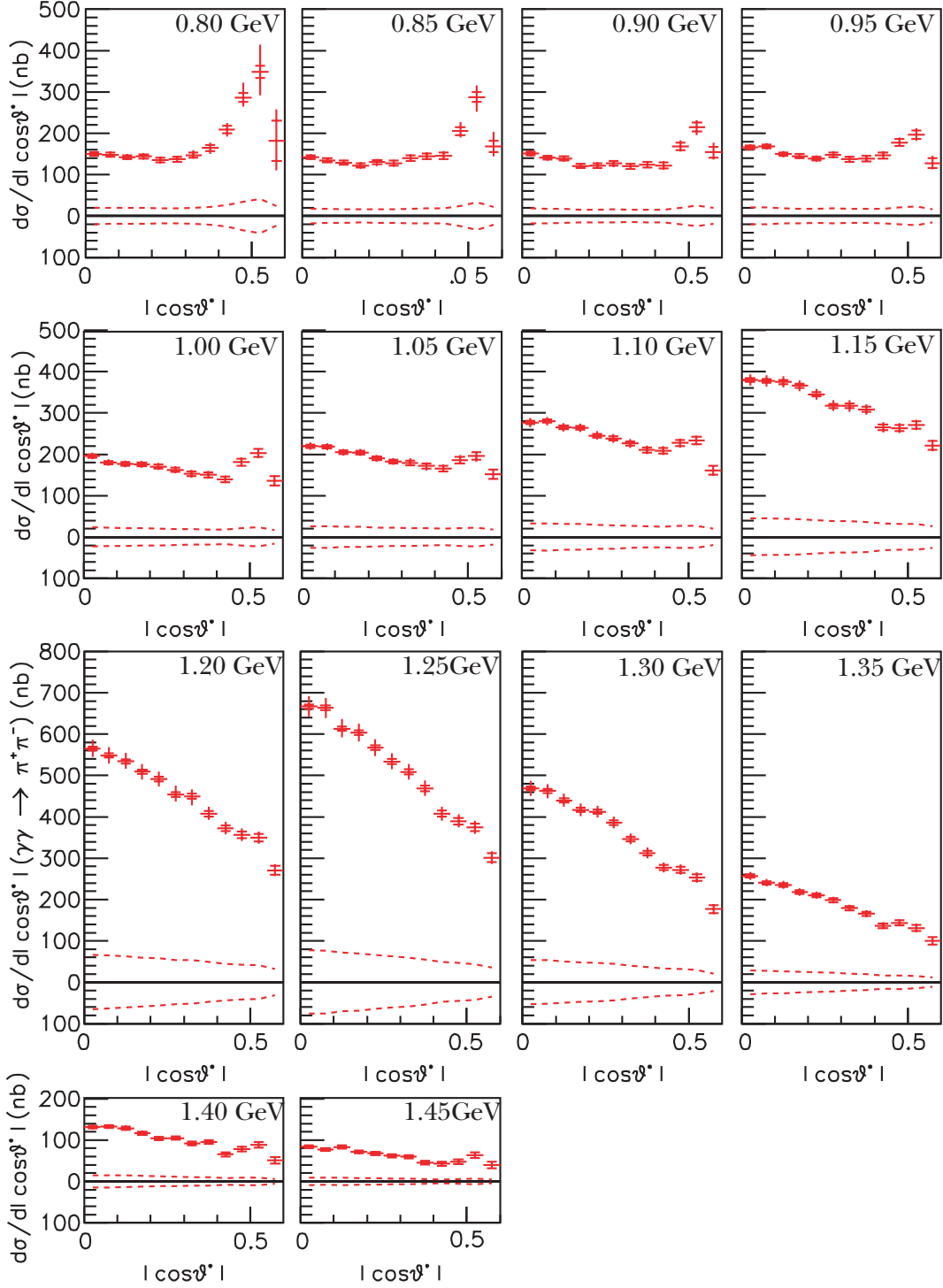


FIG. 5: Representative differential cross sections ($d\sigma/d|\cos\theta^*|$ (nb)). In the figures, 0.80 GeV means a bin of $0.800 \text{ GeV}/c^2 < W < 0.805 \text{ GeV}/c^2$, etc., and the dashed lines indicate the upper and lower overall systematic errors. The two short horizontal bars indicate the statistical errors while the vertical ones include point-by-point systematic errors.

In this W region, $J > 2$ partial waves (the next one is $J = 4$) may be neglected so that

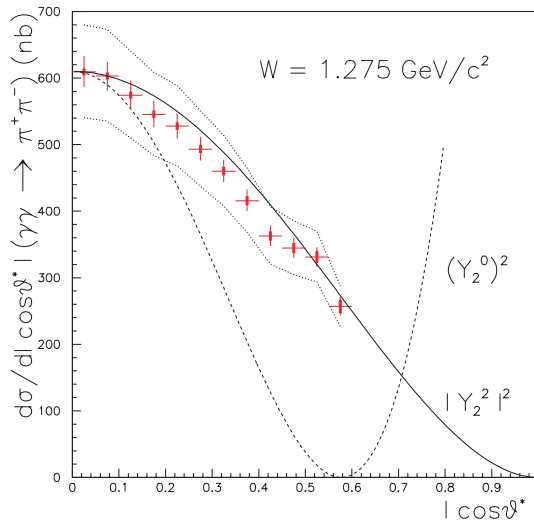


FIG. 6: The differential cross section of $\gamma\gamma \rightarrow \pi^+\pi^-$ at the $f_2(1270)$ mass ($1.275 \text{ GeV}/c^2$). Thick vertical bars show statistical errors and thin ones include point-by-point errors. The dotted lines indicate the overall systematic errors. The solid line shows the angular dependence of Y_2^2 and the dashed one shows that of Y_2^0 (both normalized at $\cos\theta^* = 0$).

only S and D waves are to be considered. The differential cross section can be expressed as:

$$\frac{d\sigma}{d\Omega}(\gamma\gamma \rightarrow \pi^+\pi^-) = |S Y_0^0 + D_0 Y_2^0|^2 + |D_2 Y_2^2|^2, \quad (4)$$

where D_0 (D_2) denotes the helicity 0 (2) component of the D wave and Y_J^m are the spherical harmonics:

$$Y_0^0 = \sqrt{\frac{1}{4\pi}}, \quad Y_2^0 = \sqrt{\frac{5}{16\pi}}(3\cos^2\theta^* - 1), \quad |Y_2^2| = \sqrt{\frac{15}{32\pi}}\sin^2\theta^*. \quad (5)$$

Since $|Y_2^2|$ is not independent of Y_2^0 and Y_0^0 (i.e. $|Y_2^2| = (\sqrt{5}Y_0^0 - Y_2^0)/\sqrt{6}$), partial waves cannot be separated from the differential cross sections alone; additional inputs or assumptions are needed. The general trend of the angular distribution as a function of W is as follows. The angular distribution below $1 \text{ GeV}/c^2$ is rather flat for $|\cos\theta^*| \leq 0.4$, indicating that the S wave fraction is significant (Fig. 5). In the region above $1 \text{ GeV}/c^2$, the angular dependence becomes steeper as W increases and is the steepest around the $f_2(1270)$ mass. Such behavior is typical of D wave dominance. Theoretically, the helicity=2 wave (D_2) is expected to be dominant [19]. This is supported by Fig. 6, where the angular dependence of $|Y_2^2|^2$ and $(Y_2^0)^2$ is plotted at the $f_2(1270)$ mass.

B. Total Cross Section

The total cross section is then obtained by integrating the differential cross sections over $|\cos\theta^*|$ up to 0.6 and is shown in Fig. 7 together with the results of some past experiments. A clear peak corresponding to the $f_0(980)$ meson is visible, indicating that the peak solution of the BP analysis is preferred. Systematic errors for the total cross section are summarized in Table I. They are dominated by the uncertainty in the μ/π separation and that of the trigger efficiency. Systematic errors arising from the μ/π separation are estimated by changing the value of $P_{\pi\pi \rightarrow \mu\mu}$ in the allowable range in each angular bin. Since $\mu^+\mu^-$ events are well identified by the KLM for $W > 1.6 \text{ GeV}$, the allowable range is determined in this

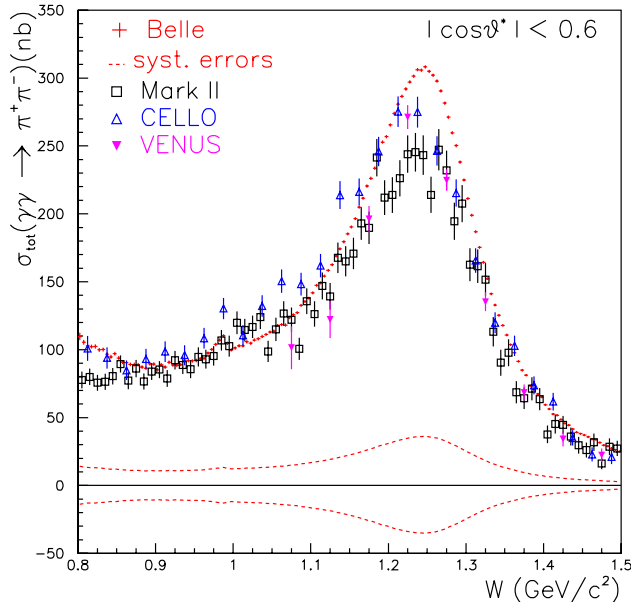


FIG. 7: The total cross section of $\gamma\gamma \rightarrow \pi^+\pi^-$ between 0.8 and 1.5 GeV/c^2 for $|\cos\theta^*| < 0.6$. The Belle data are represented by crosses with statistical error bars, the Mark II data are squares, the CELLO data are the open triangles and the VENUS data are the filled triangles. Dashed lines indicate upper and lower systematic uncertainties for the Belle data. Numerical values are listed in Appendix B. We do not show systematic errors for the other experiments; they are of similar size or larger.

region. These well identified $\mu^+\mu^-$ events are also used in estimating systematic errors of the trigger efficiency. Comparing data and MC for $\mu^+\mu^-$ events in the region $W > 1.6 \text{ GeV}$ and extrapolating linearly downward, the systematic errors are found to be 4% at $W = 1.5 \text{ GeV}$ and 10% at $W = 0.8 \text{ GeV}$. The total systematic error is obtained by summing the systematic errors in quadrature and is also shown in Fig. 7. Our results are in good agreement with past experiments except for the $f_2(1270)$ mass peak region, where our data points are about 10 to 15% larger, but still within the systematic errors.

TABLE I: Summary of systematic errors for the $\gamma\gamma \rightarrow \pi^+\pi^-$ cross section. A range is shown when the uncertainty has W dependence.

Parameter	Syst. error (%)
Tracking efficiency	2.4
Trigger efficiency	4 - 10
K/π -separation	0 - 1
μ/π -separation	5 - 7
Luminosity function	5
Integrated luminosity	1.4
Total	11.1 - 12.3

VII. FITS TO THE CROSS SECTIONS

The results of the cross section measurements can be used to obtain the parameters of $f_0(980)$ and $f_2(1270)$ resonances, and to search for other states decaying into $\pi^+\pi^-$. Some of us plan to perform a full amplitude analysis in the near future using the present data including the differential cross sections along with published cross section data of the past. Thus, we restrict our analysis to a simple level in this paper. In this section, we summarize the measurement of the parameters of the $f_0(980)$ discussed in a separate paper [14], perform a simple fit for the $f_2(1270)$ resonance as a consistency check, and search for P - and CP -violating decay of the $\eta'(958)$ meson into a $\pi^+\pi^-$ pair.

A. The $f_0(980)$ Resonance

We have to take into account the effect of the $K\bar{K}$ channel that opens within the $f_0(980)$ mass region. The fitting function for the scalar resonance $f_0(980)$ is parameterized as follows:

$$\sigma = \left| \mathcal{F}^{f_0} e^{i\varphi} + \sqrt{\sigma_0^{\text{BG}}} \right|^2 + \sigma^{\text{BG}} - \sigma_0^{\text{BG}}, \quad (6)$$

where \mathcal{F}^{f_0} is the amplitude of the $f_0(980)$ meson [20], which interferes with the helicity-0-background amplitude $\sqrt{\sigma_0^{\text{BG}}}$ with a relative phase φ , and σ^{BG} is the total background cross section. The amplitude \mathcal{F}^{f_0} can be written as

$$\mathcal{F}^{f_0} = \frac{\sqrt{4.8\pi\beta_\pi}}{W} \cdot \frac{g_{f_0\gamma\gamma}g_{f_0\pi\pi}}{16\pi} \cdot \frac{1}{D_{f_0}}, \quad (7)$$

where the factor 4.8 includes the fiducial angular acceptance $|\cos\theta^*| < 0.6$, $\beta_X = \sqrt{1 - \frac{4m_X^2}{W^2}}$ is the velocity of the particle X with mass m_X in the two-body final state $X\bar{X}$, and g_{f_0XX} is related to the partial width of the $f_0(980)$ meson via $\Gamma_{XX}(f_0) = \frac{\beta_X g_{f_0XX}^2}{16\pi m_{f_0}}$. The factor D_{f_0} is given as follows [21]:

$$D_{f_0}(W) = m_{f_0}^2 - W^2 + \Re\Pi_\pi^{f_0}(m_{f_0}) - \Pi_\pi^{f_0}(W) + \Re\Pi_K^{f_0}(m_{f_0}) - \Pi_K^{f_0}(W), \quad (8)$$

where for $X = \pi$ or K , $\Re\Pi_X^{f_0}(m_{f_0})$ is the real part of $\Pi_X^{f_0}(m_{f_0})$, which is given by:

$$\Pi_X^{f_0}(W) = \frac{\beta_X g_{f_0XX}^2}{16\pi} \left[i + \frac{1}{\pi} \ln \frac{1 - \beta_X}{1 + \beta_X} \right]. \quad (9)$$

The phase factor β_K is real in the region $W \geq 2m_K$ and becomes imaginary for $W < 2m_K$. The mass difference between K^\pm and K^0 (\bar{K}^0) is included by taking $\beta_K = \frac{1}{2}(\beta_{K^\pm} + \beta_{K^0})$.

The results of the fit (shown in Fig. 8 and in Table II) are discussed in a separate paper [14]. For completeness we report here the parameters of the $f_0(980)$ meson obtained from the fit.

$$\begin{aligned} m_{f_0} &= 985.6_{-1.5}^{+1.2} \text{ (stat)} \quad {}_{-1.6}^{+1.1} \text{ (syst)} \text{ MeV}/c^2 \\ \Gamma_{\pi^+\pi^-}(f_0) &= 34.2_{-11.8}^{+13.9} \text{ (stat)} \quad {}_{-2.5}^{+8.8} \text{ (syst)} \text{ MeV} \\ \Gamma_{\gamma\gamma}(f_0) &= 205_{-83}^{+95} \text{ (stat)} \quad {}_{-117}^{+147} \text{ (syst)} \text{ eV}. \end{aligned}$$

The two-photon width given by the PDG [2] is $\Gamma_{\gamma\gamma}(f_0) = 310_{-110}^{+80}$ (stat) eV, and the value found by BP is 280_{-130}^{+90} eV. Our value of the two-photon width is consistent with them within errors.

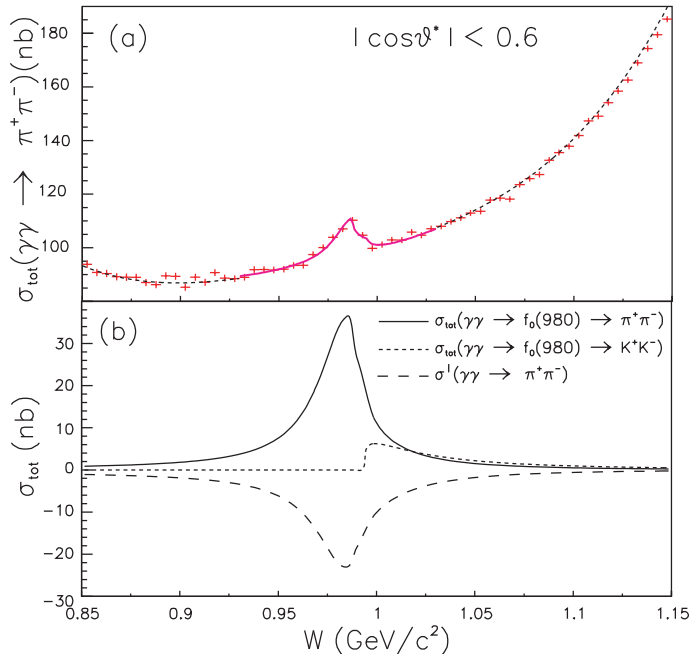


FIG. 8: Results of the fit: (a) the total cross section (the solid curve) (b) contributions of the resonance ($\sigma(\gamma\gamma \rightarrow f_0(980) \rightarrow \pi^+\pi^-)$) (solid line) and the interference (dashed). The cross section of $\sigma(\gamma\gamma \rightarrow f_0(980) \rightarrow K^+K^-)$ is also shown (dotted) [14].

TABLE II: Fitted parameters of the $f_0(980)$ region to Eq.(6).

parameter	value	error	
		stat	syst
m_{f_0} (MeV/ c^2)	985.6	+1.2 -1.5	+1.1 -1.6
$g_{\pi\pi}$ (GeV)	1.33	+0.27 -0.23	+0.16 -0.05
$\Gamma_{\gamma\gamma}(f_0)$ (eV)	205	+95 -83	+147 -117
σ_0^{BG} (nb)	3.7	+1.2 -1.5	+4.3 -3.9
φ (rad)	1.74	± 0.09	+0.04 -0.34
χ^2/ndf (ndf)	0.90 (15)		

B. The $f_2(1270)$ Region

From the past experiments [4, 5, 6, 7, 8, 9, 10], it is well known that the position of the $f_2(1270)$ resonance peak in two-photon production is shifted to lower mass because of interference with non-resonant background [22]. In this paper, we give the result of a simple fit made as a consistency check in the $f_2(1270)$ region. The relativistic Breit-Wigner resonance amplitude $A_R(W)$ for a spin- J resonance R of mass m_R is given by

$$A_R^J(W) = \sqrt{\frac{8\pi(2J+1)F_J m_R}{W}} \times \frac{\sqrt{\Gamma_{\gamma\gamma}(W)\Gamma_{\pi^+\pi^-}(W)}}{m_R^2 - W^2 - im_R\Gamma_{\text{tot}}(W)}, \quad (10)$$

where F_J is the factor coming from the limited solid angle ($|\cos\theta^*| < 0.6$). Hereafter we consider the case $J = 2$ (the $f_2(1270)$ meson). The factor $F_2 = 0.884$ is obtained assuming helicity-2 dominance [19]; the angular dependence is assumed to be Y_2^2 . The

energy-dependent total width $\Gamma_{\text{tot}}(W)$ is given by

$$\Gamma_{\text{tot}}(W) = \sum_X \Gamma_{X\bar{X}}(W), \quad (11)$$

where X is π , K , γ , etc. The partial width $\Gamma_{X\bar{X}}(W)$ is parameterized as [23]:

$$\Gamma_{X\bar{X}}(W) = \Gamma_R \mathcal{B}(R \rightarrow X\bar{X}) \left(\frac{q_X(W^2)}{q_X(m_R^2)} \right)^5 \frac{D_2(q_X(W^2)r_R)}{D_2(q_X(m_R^2)r_R)}, \quad (12)$$

where Γ_R is the total width at the resonance mass, $q_X(W^2) = \sqrt{W^2/4 - m_X^2}$, $D_2(x) = 1/(9 + 3x^2 + x^4)$, and r_R is an effective interaction radius that varies from 1 GeV^{-1} to 7 GeV^{-1} in different hadronic reactions [24]. For $X = \pi$, K , and γ , the branching fractions are $0.848_{-0.013}^{+0.025}$, 0.046 ± 0.004 , and $(1.41 \pm 0.13) \times 10^{-5}$, respectively [2]. For the 4π and the other decay modes, $\Gamma_{4\pi}(W) = \Gamma_R \mathcal{B}(R \rightarrow 4\pi) \frac{W^2}{m_R^2}$ is used instead of Eq. (12).

The fitting function for the $f_2(1270)$ region is taken to be as follows:

$$\sigma = \left| A_R^{J=2}(W) e^{i\phi_2} + b_0 \left(\frac{W}{1 \text{ GeV}/c^2} \right)^{-b_1} \right|^2 + c_0 + c_1 W + c_2 W^2, \quad (13)$$

where the contribution other than that of the $f_2(1270)$ resonance is subdivided into the interfering part (helicity=2) and the non-interfering part (helicity=0). The fit region is chosen to be $\pm\Gamma_{\text{tot}}$ around the f_2 mass, i.e. $1.090 \text{ GeV}/c^2 < W < 1.461 \text{ GeV}/c^2$. The parameters of the $f_2(1270)$ meson are fixed to the values from the PDG: the branching fractions as listed above, $m_R = 1275.4 \pm 1.1 \text{ MeV}/c^2$ and $\Gamma_R = 185.2_{-2.5}^{+3.1} \text{ MeV}$ [2], and the parameter r_R is floated.

The result of the fit is shown in Fig. 9 and the obtained parameters are summarized in Table III, where errors shown are statistical only. Since a good fit is obtained with $c_2 = 0$, we omit c_2 . A fit without the non-interfering background gives much worse results as summarized in Table III. We conclude that the consistency check is satisfactory.

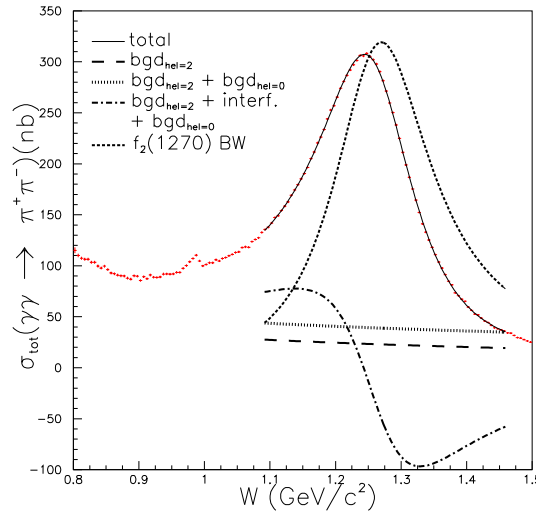


FIG. 9: Results of the fit of the $f_2(1270)$ region to Eq. (13). The parameters of the $f_2(1270)$ mesons are fixed to the values by the PDG (with the helicity=0 background).

TABLE III: Fitted parameters for the $f_2(1270)$ region to Eq. (13). The parameters of the $f_2(1270)$ meson are fixed to the values by the PDG. Errors shown are statistical only.

parameter	with hel.=0 bgd	without hel.=0 bgd
r_R (GeV^{-1})	3.62 ± 0.03	2.84 ± 0.04
b_0 ($\sqrt{\text{nb}}$)	5.54 ± 0.02	7.70 ± 0.05
b_1	0.61 ± 0.05	2.00 ± 0.02
ϕ_2 (deg.)	28.7 ± 0.2	22.8 ± 0.1
c_0 (nb)	18.2 ± 3.7	0 (fixed)
c_1 (nb/ GeV/c^2)	-1.7 ± 2.8	0 (fixed)
c_2 (nb/ $(\text{GeV}/c^2)^2$)	0 (fixed)	0 (fixed)
χ^2/ndf (ndf)	1.1 (68)	2.1 (70)

C. The $\pi^+\pi^-$ branching fraction of the η' (958) meson

The η' (958) meson is a pseudoscalar meson and, thus, its coupling to $\pi\pi$ violates P and CP . The present upper limit for the $\pi^+\pi^-$ branching fraction $\mathcal{B}(\eta' \rightarrow \pi^+\pi^-)$ is 2% [25]. The high statistics data of Belle allow for a more sensitive search. The η' (958) meson has a small width of $\Gamma_{\eta'} = 0.202 \pm 0.016$ MeV and a mass of $m_{\eta'} = 957.78 \pm 0.14$ MeV/ c^2 . Thus its contribution to the W spectrum can be represented by a Gaussian function:

$$f_{\eta'}(W)dW = \frac{S_{\eta'}}{\sqrt{2\pi}\sigma_W} \exp\left(-\frac{(W - m_{\eta'})^2}{2\sigma_W^2}\right) dW, \quad (14)$$

where $S_{\eta'}$ is the parameter to be determined, and $\sigma_W = 2.0 \pm 0.2$ MeV/ c^2 is the mass resolution determined from MC. The total cross section in the region 0.92 GeV/ $c^2 \leq W \leq 0.98$ GeV/ c^2 is fitted with a second-order polynomial plus Eq. (14). The finite bin-size effect is taken into account by integrating the Gaussian over each bin. The result is $S_{\eta'} = -27 \pm 16$ nb \cdot MeV. The systematic error is found to be negligible, which is estimated by constraining the η' mass and the mass resolution within one standard deviation and by changing the fitting region.

The parameter $S_{\eta'}$ can be related to the $\pi^+\pi^-$ branching fraction $\mathcal{B}(\eta' \rightarrow \pi^+\pi^-)$ as follows. The cross section formula to be used is the same as Eq. (6) except for replacing the amplitude \mathcal{F}^{f_0} by Eq. (10) with $J = 0$:

$$\sqrt{\frac{4.8\pi m_{\eta'}}{W} \frac{\sqrt{\Gamma_{\eta'}\Gamma_{\gamma\gamma}\mathcal{B}(\eta' \rightarrow \pi^+\pi^-)}}{M_{\eta'}^2 - W^2 - im_{\eta'}\Gamma_{\eta'}}} \simeq -\frac{\sqrt{4.8\pi\Gamma_{\eta'}\Gamma_{\gamma\gamma}\mathcal{B}(\eta' \rightarrow \pi^+\pi^-)}}{2m_{\eta'}(W - m_{\eta'} + i\frac{\Gamma_{\eta'}}{2})}, \quad (15)$$

where $\Gamma_{\gamma\gamma} = 4.30 \pm 0.15$ keV [2] is the two-photon width of the η' meson, and the latter equation is obtained in a narrow width approximation. Taking into account an interference effect (for the most conservative case) and using the relation $\int_0^\infty dW/((W - m_{\eta'})^2 + \Gamma_{\eta'}^2/4) \simeq 2\pi/\Gamma_{\eta'}$, we obtain:

$$S_{\eta'} = \frac{1.2\pi}{m_{\eta'}} \left(\frac{2\pi\Gamma_{\gamma\gamma}\mathcal{B}(\eta' \rightarrow \pi^+\pi^-)}{m_{\eta'}} + \sin\varphi' \sqrt{2\pi\sigma_0^{\text{BG}}\Gamma_{\eta'}\Gamma_{\gamma\gamma}\mathcal{B}(\eta' \rightarrow \pi^+\pi^-)} \right), \quad (16)$$

where σ_0^{BG} is the cross section of the continuum $\gamma\gamma \rightarrow \pi^+\pi^-$ component whose amplitude interferes with the P - and CP -violating η' decay, and φ' is the phase angle and $\sin\varphi' = -1$ gives the most conservative upper limit of $S_{\eta'}$.

To obtain the upper limit for $S_{\eta'}$ at 90% confidence level (C.L.), we have to consider two physically possible cases: $S_{\eta'}$ is negative or positive, depending on the presence or absence of an interference effect between amplitudes of opposite P and CP . As the reaction

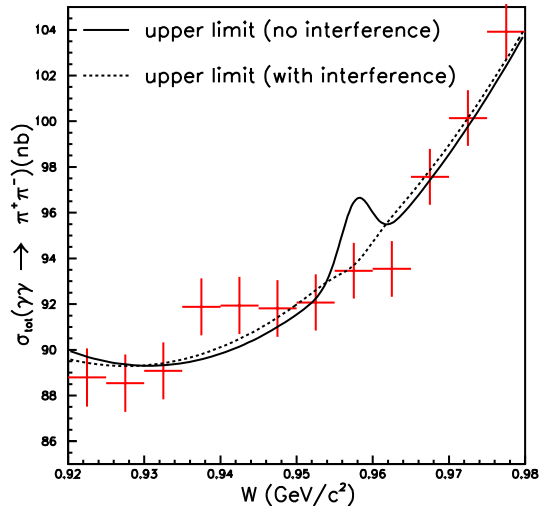


FIG. 10: Fit result of a Gaussian + second-order polynomial in the $\eta'(958)$ region. The solid (dotted) line is the 90% C.L. upper limit without (with) interference.

$\gamma\gamma \rightarrow \eta'$ would take place via a P wave, while only even orbital angular momentum waves can contribute to the ordinary $\gamma\gamma \rightarrow \pi^+\pi^-$ process, it is unlikely that these two processes would interfere. In that case, $\sigma_0^{\text{BG}} = 0$ and $S_{\eta'}$ is non negative. On the other hand, if interference is present, the lowest boundary of $S_{\eta'}$ is $-\pi\sigma_0^{\text{BG}}\Gamma_{\eta'}/2 \simeq -30 \text{ nb}\cdot\text{MeV}$, where $\sigma_0^{\text{BG}} = 93.5 \text{ nb}$ is used, i.e. the largest possible value of σ_0^{BG} that gives the most conservative limit.

We first obtain $S_{\eta'}^{90}$, the 90% C.L. upper limit of $S_{\eta'}$ from the following relation:

$$\int_{S_{\eta'}^{\text{min}}}^{S_{\eta'}^{90}} \exp\left(-\frac{\chi^2(S_{\eta'})}{2}\right) dS_{\eta'} = 0.9 \int_{S_{\eta'}^{\text{min}}}^{\infty} \exp\left(-\frac{\chi^2(S_{\eta'})}{2}\right) dS_{\eta'}, \quad (17)$$

where $\chi^2(S_{\eta'})$ is the χ^2 from the fit with a fixed $S_{\eta'}$ and $S_{\eta'}^{\text{min}}$ is the lower physical boundary of $S_{\eta'}$. In the presence (absence) of the interference effect, the limit is determined to be $S_{\eta'}^{90} < -2.0$ ($S_{\eta'}^{90} < 14.4$) $\text{nb}\cdot\text{MeV}$. The results are shown in Fig. 10. We obtain the upper limit of $\mathcal{B}(\eta' \rightarrow \pi^+\pi^-)$ taking the errors of $\Gamma_{\gamma\gamma}$ and $\mathcal{B}_{\gamma\gamma}$ ($\equiv \Gamma_{\gamma\gamma}/\Gamma_{\eta'}$) into account. Namely, we calculate the contribution to the uncertainty in $S_{\eta'}$ that arises from these parameters and combine it with the statistical error of $S_{\eta'}$, $16 \text{ nb}\cdot\text{MeV}$, reevaluate $S_{\eta'}^{90}$, and then translate it into a limit for $\mathcal{B}(\eta' \rightarrow \pi^+\pi^-)$. In the case of no interference, we obtain $\mathcal{B}(\eta' \rightarrow \pi^+\pi^-) < 3.3 \times 10^{-4}$. In the other extreme case of maximum interference, we use $\sigma_0^{\text{BG}} = 93.5 \text{ nb}$, and the limit is $\mathcal{B}(\eta' \rightarrow \pi^+\pi^-) < 2.8 \times 10^{-3}$ at 90% C.L. The errors in $\Gamma_{\gamma\gamma}$ and $\mathcal{B}_{\gamma\gamma}$ are also included but they lead to a negligible change in the upper limits.

VIII. SUMMARY AND CONCLUSION

In summary, we have performed a high statistics measurement of the $\gamma\gamma \rightarrow \pi^+\pi^-$ cross sections in the $\pi^+\pi^-$ invariant mass region $0.80 \text{ GeV}/c^2 \leq W \leq 1.5 \text{ GeV}/c^2$ for $|\cos\theta^*| < 0.6$ with the Belle detector at the KEKB e^+e^- collider. The total cross section is measured in fine bins of W ($\Delta W = 5 \text{ MeV}/c^2$) and differential cross sections are given in bins of $\Delta W = 5 \text{ MeV}/c^2$ and $\Delta|\cos\theta^*| = 0.05$. We have observed a significant peak corresponding to the $f_0(980)$ resonance. Our data clearly select the peak solution of the Boglione-Pennington amplitude analysis [11]. The total cross section is fitted to obtain the parameters of the

$f_0(980)$ meson [14] and to check consistency in the $f_2(1270)$ region. For a P - and CP -violating decay of the $\eta'(958)$ meson, we set an upper limit without (with) interference between opposite P and CP amplitudes $\mathcal{B}(\eta'(958) \rightarrow \pi^+\pi^-) < 3.3 \times 10^{-4}$ ($< 2.9 \times 10^{-3}$) at 90% C.L. thereby significantly improving the previous limit of 0.02 [2]. The angular dependence of the differential cross sections is consistent with the presence of a significant S wave fraction for $W \lesssim 1 \text{ GeV}/c^2$ and with the dominance of the D wave in the $f_2(1270)$ mass region.

Acknowledgment

We are indebted to M. Pennington for various enlightening discussions and useful suggestions. We thank the KEKB group for the excellent operation of the accelerator, the KEK cryogenics group for the efficient operation of the solenoid, and the KEK computer group and the National Institute of Informatics for valuable computing and Super-SINET network support. We acknowledge support from the Ministry of Education, Culture, Sports, Science, and Technology of Japan and the Japan Society for the Promotion of Science; the Australian Research Council and the Australian Department of Education, Science and Training; the National Science Foundation of China and the Knowledge Innovation Program of the Chinese Academy of Sciences under contract No. 10575109 and IHEP-U-503; the Department of Science and Technology of India; the BK21 program of the Ministry of Education of Korea, the CHEP SRC program and Basic Research program (grant No. R01-2005-000-10089-0) of the Korea Science and Engineering Foundation, and the Pure Basic Research Group program of the Korea Research Foundation; the Polish State Committee for Scientific Research; the Ministry of Education and Science of the Russian Federation and the Russian Federal Agency for Atomic Energy; the Slovenian Research Agency; the Swiss National Science Foundation; the National Science Council and the Ministry of Education of Taiwan; and the U.S. Department of Energy.

APPENDIX A: BACKGROUND SUBTRACTION

In this section, we describe in detail how the background from $\eta' \rightarrow \pi^+\pi^-\gamma$ is subtracted in the cross section determinations described in Section VI and Appendix B. Note that beam-gas background that was important in past experiments is completely negligible at B -factories because of the very high luminosity. The dominant physics background is due to $\eta'(958)$ production and its subsequent decay into $\rho^0\gamma$; the photon energy at the nominal ρ^0 mass is 0.14 GeV, and a significant fraction of $\pi^+\pi^-$ pairs satisfy selection requirements such as $|\sum \mathbf{p}_t^*| < 0.1 \text{ GeV}/c$. The other physics backgrounds are negligibly small.

The background from $\eta' \rightarrow \pi^+\pi^-\gamma$ can be estimated with MC at the four-vector level without doing a full detector simulation. This is because the subtractions are applied to cross sections where efficiency corrections of the detector and trigger are already included and because the bin-sizes used are large enough that the effect of finite detector resolution is negligible. The process $e^+e^- \rightarrow e^+e^-\eta'$ with $\eta' \rightarrow \rho^0\gamma \rightarrow \pi^+\pi^-\gamma$ is simulated using TREPS [17]. The final state $\pi^+\pi^-\gamma$ is generated with a matrix element incorporating the dipole transition feature of the $\eta' \rightarrow \rho^0\gamma$ decay and the ρ pole [25, 26]:

$$|\mathcal{M}(m_{\pi^+\pi^-}, E_\gamma, \theta)|^2 \propto \frac{p_\pi^2 E_\gamma^2 m_{\pi^+\pi^-}^2 \sin^2 \theta}{(m_\rho^2 - m_{\pi^+\pi^-}^2)^2 + m_\rho^2 \Gamma^2(m_{\pi^+\pi^-})}, \quad (\text{A1})$$

where p_π is the pion momentum, E_γ is the photon energy and θ is the angle between one of the pions and the photon, all evaluated in the di-pion rest system, and the denominator is

the ρ pole. The mass dependence of the ρ width is parameterized as [27]:

$$\Gamma(m) = \frac{2p_\pi^3}{p_0(p_\pi^2 + p_0^2)}\Gamma_0, \quad (\text{A2})$$

where p_0 is the p_π at $m = m_\rho$ and Γ_0 is the nominal ρ width. Generated $\pi^+\pi^-$ pairs are subjected to the cut $|\sum \mathbf{p}_t^*| < 0.1 \text{ GeV}/c$ and then accumulated into bins of $W - |\cos\theta^*|$ with the same bin size as that of the differential cross sections. The obtained distribution is related to the cross section of $\gamma\gamma \rightarrow X$ by using [18]:

$$d\sigma(e^+e^- \rightarrow e^+e^-X) = dW \frac{d\mathcal{L}}{dW}(W)\sigma(\gamma\gamma \rightarrow X). \quad (\text{A3})$$

The resulting background cross sections to be subtracted are shown in Figs. 11(a) and (b).

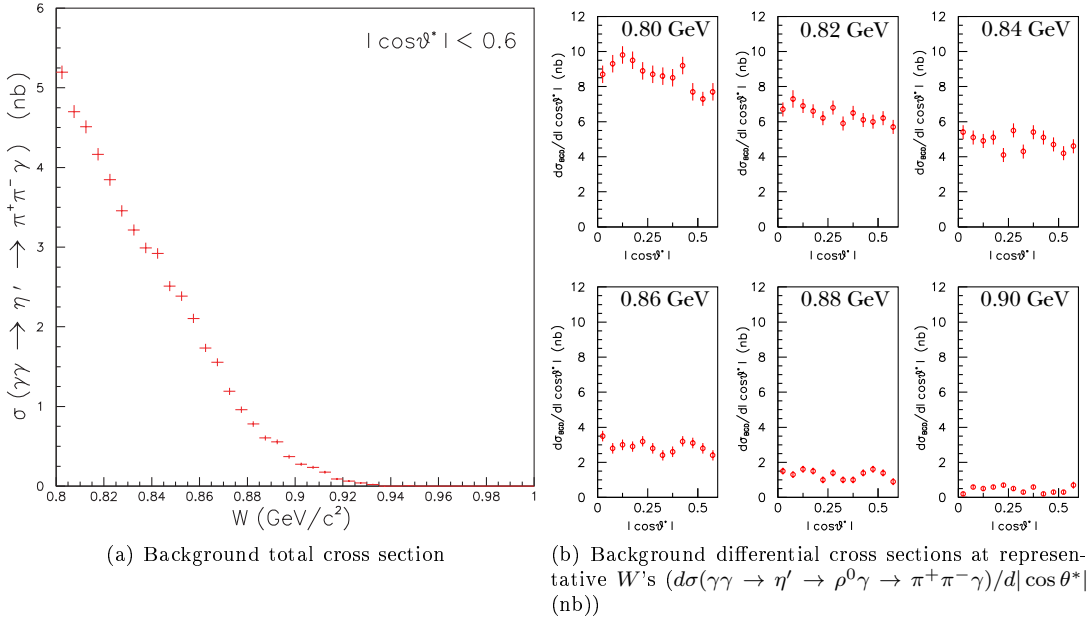


FIG. 11: Background total and differential cross sections ($\gamma\gamma \rightarrow \eta' \rightarrow \rho^0\gamma \rightarrow \pi^+\pi^-\gamma$)

APPENDIX B: TOTAL CROSS SECTION

In this appendix, we list the measured values of the total cross section for the process $\gamma\gamma \rightarrow \pi^+\pi^-$ integrated over the angular region $|\cos\theta^*| < 0.6$ in the range of $0.8 \text{ GeV}/c^2 < W < 1.5 \text{ GeV}/c^2$ in steps of $\Delta W = 0.005 \text{ GeV}/c^2$. At each energy, the third number in the table is the statistical and the fourth is the overall systematic error.

W GeV/ c^2	σ nb	stat nb	syst nb	W GeV/ c^2	σ nb	stat nb	syst nb	W GeV/ c^2	σ nb	stat nb	syst nb	W GeV/ c^2	σ nb	stat nb	syst nb
0.8025	109.74	2.77	+14.15 -13.90	0.8075	105.40	1.80	+13.55 -13.30	0.8125	102.85	1.54	+13.21 -12.97	0.8175	102.25	1.52	+13.13 -12.87
0.8225	102.40	1.48	+13.08 -12.83	0.8275	99.89	1.44	+12.77 -12.51	0.8325	100.11	1.43	+12.71 -12.47	0.8375	96.69	1.41	+12.30 -12.05
0.8425	94.74	1.39	+12.06 -11.82	0.8475	97.08	1.38	+12.19 -11.96	0.8525	93.85	1.37	+11.82 -11.58	0.8575	90.78	1.36	+11.46 -11.22
0.8625	90.40	1.36	+11.35 -11.11	0.8675	89.21	1.35	+11.18 -10.95	0.8725	89.02	1.35	+11.10 -10.87	0.8775	88.96	1.34	+11.05 -10.82
0.8825	87.07	1.33	+10.83 -10.60	0.8875	86.25	1.32	+10.71 -10.48	0.8925	89.55	1.32	+11.02 -10.79	0.8975	89.37	1.31	+11.05 -10.97
0.9025	85.27	1.30	+10.56 -10.32	0.9075	89.03	1.30	+10.91 -10.69	0.9125	87.14	1.28	+10.72 -10.49	0.9175	90.73	1.28	+11.06 -10.84
0.9225	88.69	1.27	+10.86 -10.63	0.9275	88.47	1.26	+10.84 -10.60	0.9325	89.00	1.25	+10.89 -10.65	0.9375	91.84	1.25	+11.18 -10.93
0.9425	91.88	1.25	+11.20 -10.95	0.9475	91.74	1.24	+11.20 -10.95	0.9525	92.02	1.23	+11.26 -10.99	0.9575	93.41	1.22	+11.42 -11.16
0.9625	93.48	1.22	+11.47 -11.19	0.9675	97.46	1.22	+11.90 -11.62	0.9725	100.08	1.22	+12.17 -11.89	0.9775	103.87	1.21	+12.57 -12.29
0.9825	107.07	1.21	+12.90 -12.62	0.9875	110.24	1.21	+13.21 -12.89	0.9925	104.68	1.19	+12.63 -12.40	0.9975	99.79	1.18	+12.23 -11.87
1.0025	101.21	1.17	+12.36 -12.06	1.0075	102.91	1.17	+12.51 -12.21	1.0125	102.86	1.16	+12.51 -12.21	1.0175	105.85	1.16	+12.80 -12.50
1.0225	104.71	1.15	+12.70 -12.39	1.0275	107.10	1.15	+12.94 -12.64	1.0325	108.03	1.14	+13.06 -12.75	1.0375	109.75	1.14	+13.25 -12.94
1.0425	111.16	1.14	+13.42 -13.10	1.0475	112.96	1.14	+13.62 -13.30	1.0525	113.58	1.13	+13.72 -13.39	1.0575	117.81	1.13	+14.16 -13.83
1.0625	118.50	1.13	+14.27 -13.93	1.0675	118.14	1.12	+14.29 -13.93	1.0725	123.57	1.13	+14.85 -14.49	1.0775	125.80	1.12	+15.12 -14.75
1.0825	127.32	1.12	+15.33 -14.95	1.0875	132.64	1.12	+15.90 -15.51	1.0925	135.50	1.12	+16.25 -15.85	1.0975	137.82	1.12	+16.55 -16.14
1.1025	141.86	1.12	+17.01 -16.59	1.1075	147.31	1.12	+17.60 -17.17	1.1125	149.05	1.12	+17.86 -17.41	1.1175	154.11	1.13	+18.43 -17.97
1.1225	158.42	1.13	+18.94 -18.47	1.1275	162.55	1.13	+19.45 -18.95	1.1325	168.98	1.14	+20.16 -19.66	1.1375	174.29	1.14	+20.79 -20.27
1.1425	179.45	1.14	+21.41 -20.87	1.1475	185.23	1.15	+22.09 -21.53	1.1525	190.32	1.15	+22.72 -22.13	1.1575	196.50	1.15	+23.45 -22.83
1.1625	205.00	1.16	+24.40 -23.76	1.1675	211.52	1.17	+25.18 -24.52	1.1725	220.50	1.17	+26.17 -25.50	1.1775	226.11	1.18	+26.88 -26.18
1.1825	233.61	1.18	+27.76 -27.04	1.1875	243.91	1.19	+28.89 -28.15	1.1925	252.79	1.20	+29.89 -29.13	1.1975	256.88	1.20	+30.46 -29.68
1.2025	265.45	1.21	+31.43 -30.62	1.2075	273.94	1.22	+32.37 -31.55	1.2125	280.81	1.23	+33.17 -32.32	1.2175	286.54	1.23	+33.85 -32.97
1.2225	291.98	1.23	+34.47 -33.57	1.2275	297.12	1.24	+35.05 -34.13	1.2325	301.35	1.24	+35.50 -34.57	1.2375	306.15	1.24	+35.98 -35.04
1.2425	305.83	1.24	+35.97 -35.01	1.2475	308.21	1.24	+36.14 -35.19	1.2525	304.94	1.24	+35.78 -34.82	1.2575	302.09	1.23	+35.40 -34.46
1.2625	297.81	1.22	+34.85 -33.93	1.2675	290.47	1.22	+33.99 -33.08	1.2725	281.53	1.20	+32.94 -32.05	1.2775	271.20	1.18	+31.73 -30.87
1.2825	259.63	1.17	+30.38 -29.55	1.2875	250.20	1.15	+29.19 -28.40	1.2925	238.08	1.14	+27.75 -27.00	1.2975	224.97	1.12	+26.21 -25.51
1.3025	211.19	1.10	+24.62 -23.95	1.3075	198.86	1.09	+23.15 -22.52	1.3125	186.77	1.07	+21.71 -21.12	1.3175	175.27	1.06	+20.34 -19.79
1.3225	164.29	1.04	+19.04 -18.52	1.3275	152.31	1.03	+17.68 -17.18	1.3325	141.10	1.01	+16.41 -15.94	1.3375	132.89	1.00	+15.42 -14.98
1.3425	125.24	0.99	+14.50 -14.09	1.3475	117.89	0.98	+13.63 -13.24	1.3525	110.82	0.96	+12.79 -12.42	1.3575	103.72	0.95	+11.96 -11.62
1.3625	97.71	0.94	+11.27 -10.93	1.3675	91.35	0.93	+10.48 -10.23	1.3725	84.87	0.92	+9.76 -9.50	1.3775	81.18	0.92	+9.29 -9.04
1.3825	73.44	0.91	+8.47 -8.23	1.3875	70.56	0.90	+8.07 -7.86	1.3925	67.25	0.90	+7.67 -7.46	1.3975	65.05	0.90	+7.36 -7.17
1.4025	59.39	0.89	+6.77 -6.59	1.4075	56.28	0.88	+6.41 -6.23	1.4125	52.53	0.87	+6.00 -5.84	1.4175	51.69	0.87	+5.85 -5.69
1.4225	48.65	0.87	+5.51 -5.36	1.4275	45.78	0.86	+5.20 -5.06	1.4325	44.40	0.86	+5.01 -4.88	1.4375	41.55	0.85	+4.71 -4.59
1.4425	39.18	0.84	+4.46 -4.34	1.4475	38.13	0.84	+4.32 -4.20	1.4525	37.14	0.85	+4.18 -4.08	1.4575	35.84	0.84	+4.03 -3.93
1.4625	34.07	0.84	+3.84 -3.74	1.4675	33.83	0.84	+3.78 -3.68	1.4725	31.64	0.83	+3.55 -3.46	1.4775	29.58	0.83	+3.34 -3.25
1.4825	29.00	0.83	+3.25 -3.16	1.4875	27.52	0.83	+3.08 -3.00	1.4925	26.25	0.82	+2.93 -2.85	1.4975	25.07	0.83	+2.79 -2.72

REFERENCES

- [1] For a review, see, e.g. C. Amsler and N.A. Törnqvist, Phys. Rep. **389**, 61 (2004).
- [2] W.-M. Yao *et al.* (PDG), J. Phys. G **33**, 1 (2006).
- [3] L.D. Landau, Sov. Phys. Dokl. **60**, 207 (1948); C.N. Yang, Phys. Rev. **77**, 242 (1950).
- [4] H. Marsiske *et al.* (Crystal Ball Collaboration), Phys. Rev. D **41**, 3324 (1990).

- [5] J. Boyer *et al.* (Mark II Collaboration), *Phys. Rev. D* **42**, 1350 (1990).
- [6] T. Oest *et al.* (JADE Collaboration), *Z. Phys. C - Particles and Fields* **47**, 343 (1990).
- [7] I. Adachi *et al.* (TOPAZ Collaboration), *Phys. Lett. B* **234**, 185 (1990).
- [8] A.E. Blinov *et al.* (MD-1 Collaboration), *Z. Phys. C - Particles and Fields* **53**, 33 (1992).
- [9] H. -J. Behrend *et al.* (CELLO Collaboration), *Z. Phys. C - Particles and Fields* **56**, 381 (1992).
- [10] F. Yabuki *et al.* (VENUS Collaboration), *J. Phys. Soc. Jpn* **64**, 435 (1995).
- [11] M. Boglione and M. R. Pennington, *Eur. Phys. J. C* **9**, 11 (1999); referred to as BP.
- [12] S. Kurokawa and E. Kikutani, *Nucl. Instrum. and Meth. A* **499**, 1 (2003), and other papers included in this volume.
- [13] The total cross section for two-photon production of $\pi^+\pi^-$ is proportional to $(\ln(E_{\text{beam}}/m_\pi))^2 \ln(E_{\text{beam}}/m_e)$ in the point-like pion approximation for $E_{\text{beam}} \gg m_\pi$, where E_{beam} is the center-of-mass beam energy of an e^+e^- collider and m_π (m_e) is the mass of the pion (electron); see, e.g. S.J. Brodsky, T. Kinoshita and H. Terazawa, *Phys. Rev. Lett.* **25**, 972 (1970). The first paper to notice the existence of the two photon process appears to be L.D. Landau and E.M. Lifshitz, *Sov. Phys. Rev.* **6**, 244 (1934).
- [14] T. Mori *et al.* (Belle Collaboration), *Phys. Rev. D* **75**, 051101(R) (2007). Note that the fitted curve in Fig. 2(a) of this published paper had a slight shift due to an error in plotting, which is corrected in Fig. 8(a) in the present paper.
- [15] A. Abashian *et al.* (Belle Collaboration), *Nucl. Instrum. and Meth. A* **479**, 117 (2002).
- [16] R. Brun *et al.*, CERN DD/EE/84-1 (1987).
- [17] S. Uehara, KEK Report 96-11 (1996).
- [18] V.M. Budnev *et al.*, *Phys. Rep.* **15**, 181 (1975).
- [19] see, e.g. H. Krasemann and J.A.M. Vermaseren, *Nucl. Phys. B* **184**, 269 (1981).
- [20] Note that the normalization of the amplitude is changed from that of Ref. [14] in order to be consistent with those for other resonances ($f_2(1270)$ and $\eta'(958)$).
- [21] S.M. Flattè, *Phys. Lett.* **63B**, 224 (1976); N.N. Achasov and G.N. Shestakov, *Phys. Rev. D* **72**, 013006 (2005).
- [22] A. Roussarie *et al.*, (Mark II Collaboration) *Phys. Lett. B* **105**, 304 (1981).
- [23] J.M. Blatt and V.F. Weiskopff, *Theoretical Nuclear Physics* (Wiley, New York, 1952), pp. 359-365 and 386-389.
- [24] G. Grayer *et al.*, *Nucl. Phys. B* **75**, 189 (1974); A. Garmash *et al.* (Belle Collaboration), *Phys. Rev. D* **71**, 092003 (2005); B. Aubert *et al.* (BaBar Collaboration), *Phys. Rev. D* **72**, 052002 (2005).
- [25] A. Rittenberg, Ph.D. Thesis, LBL, Univ. of California (1969), UURL-18863, Sec. VI.A, Table VIII.
- [26] H. Albrecht *et al.* (ARGUS Collaboration), *Phys. Lett. B* **199**, 457 (1987).
- [27] J.D. Jackson, *Nuovo Cimento* **34**,1644 (1964).